

Accepted by Cement and Concrete Composites, Dec. 2017.

Influence of Substrate Moisture State and Roughness on Interface Microstructure and Bond Strength: Slant Shear vs. Pull-Off Testing

Dale P. Bentz^A, Igor De la Varga^B, Jose F. Muñoz^B, Robert P. Spragg^B, Benjamin A. Graybeal^C, Daniel S. Hussey^D, David L. Jacobson^D, Scott Z. Jones^A, and Jacob M. LaManna^D

^AEngineering Laboratory
National Institute of Standards and Technology, Gaithersburg, MD 20899
E-mails: dale.bentz@nist.gov, scott.jones@nist.gov

^BSES Group & Associates
Federal Highway Administration, McClean, VA 22101
E-mails: igor.delavarga.ctr@dot.gov, jose.munoz.ctr@dot.gov, robert.spragg.ctr@dot.gov

^CTurner-Fairbanks Highway Research Center
Federal Highway Administration, McClean, VA 22101
E-mail: benjamin.graybeal@dot.gov

^DPhysical Measurement Laboratory
National Institute of Standards and Technology, Gaithersburg, MD 20899
E-mails: daniel.hussey@nist.gov, david.jacobson@nist.gov, jacob.lamanna@nist.gov

Abstract

There are conflicting views in the literature concerning the optimum moisture state for an existing substrate prior to the application of a repair material. Both saturated-surface-dry (SSD) and dry substrates have been found to be preferable in a variety of studies. One confounding factor is that some studies evaluate bonding of the repair material to the substrate via pull-off (direct tension) testing, while others have employed some form of shear specimens as their preferred testing configuration. Available evidence suggests that dry substrate specimens usually perform equivalently or better in shear testing, while SSD ones generally exhibit higher bond strengths when a pull-off test is performed, although exceptions to these trends have been observed. This paper applies a variety of microstructural characterization tools to investigate the interfacial microstructure that develops when a fresh repair material is applied to either a dry or SSD substrate. Simultaneous neutron and X-ray radiography are employed to observe the dynamic microstructural rearrangements that occur at this interface during the first 4 h of curing. Based on the differences in water movement and densification (particle compaction) that occur for the dry and SSD specimens, respectively, a hypothesis is formulated as to why different bond tests may favor one moisture state over the other, also dependent on their surface roughness. It is suggested that the compaction of particles at a dry substrate surface may increase the frictional resistance when tested under slant shear loading, but contribute relatively little to the bonding when the interface is submitted to pull-off forces. For maximizing bond performance, the fluidity of the repair material and the roughness and moisture state of the substrate must all be given adequate consideration.

Keywords: Bond; Densification; Interface; Moisture; Neutron Radiography; Repair Material; Roughness; Slant Shear; Tension; X-ray Radiography.

Introduction

As concrete continues to be the most widely used construction material on Earth, the needs for repair of existing concrete structures continue to expand. One critical issue in applying a repair material (RM) to an existing concrete substrate is the bond that is developed between the new and original materials. As stresses concentrate at this interface during service (due to potential elastic modulus and/or coefficient of thermal expansion mismatches and drying gradients, for example), the bond strength must be sufficient to resist curling, delamination, cracking, and spalling. Therefore, extensive recommendations concerning the preparation of the existing concrete surface prior to the application of the RMs have been developed [1-3]. While the role of surface roughness in promoting bond has been evaluated and is relatively better understood [4,5], that of the moisture content of the existing concrete substrate remains controversial [1-3,6-14]. Some authors claim that a dry substrate should be employed, as wetting the surface offers no improvement in measured bond strength and is in fact sometimes detrimental [3,6,9-10,13], others assert that a saturated-surface-dry (SSD) surface produces a superior bond and microstructure [3,11,12,14], and a third group promotes a saturation level for the surface of the existing concrete substrate of between 50 % and 90 % as being optimal for bonding [1,8].

From a theoretical viewpoint, arguments can be made for both dry and wet moisture states of the existing substrate surface as being superior. If the existing substrate surface is dry when the fresh RM is applied, it will absorb moisture from the RM, locally densifying the microstructure near the interface and potentially creating a lock-and-key type structure at the existing substrate surface, as individual particles within the RM mixture could be drawn into the nooks and crannies of the roughened substrate surface. This scenario presumes that the fresh RM itself is sufficiently fluid to flow into the nooks and crannies. After proper curing, this densified layer will potentially provide a stronger bond between repair and existing material, leading to failure under tensile or shear loading either within the bulk of the RM or the existing concrete, but not at the interfacial bond between the two. Conversely, if too much water is removed from the RM at the interface during this sorption process, insufficient water for the complete hydration of the cementitious component of the RM (and its accompanying strength development) may remain [13]. This may lead to a weak layer of (mostly unhydrated) RM being present at the interface that will become the site of premature failure upon loading under either tension or shear conditions. Such performance would not typically be expected if the existing substrate were prepared to be SSD prior to the application of the repair, effectively minimizing subsequent moisture transfer across the interface, while still perhaps aiding in consolidation of the fresh RM at this interface.

The bonding performance of RMs can be evaluated under different loading conditions [15-20], with (slant) shear and pull-off (direct tension) being two of the more common configurations (Figure 1). Using different test methods on the nominally same materials can produce measured bond strengths that vary by up to a factor of 8 [17]. Furthermore, there are some indications that the influence of surface moisture on bond performance depends on whether the test is assessing the shear or the tensile strength of the interface [8]. Results obtained by the present authors [10,14] have also highlighted this difference, with slant shear testing usually indicating that dry specimens produce stronger bonding, while the converse is generally true for pull-off testing. Of course, it must be recognized that these past studies were conducted using different substrate materials, even when a subset of the RMs were identical. The objective of the present paper is to examine this performance difference in some detail, particularly with respect to its

relationship to the microstructure formed within the interfacial region as a function of the substrate moisture state (and surface roughness as a secondary variable).

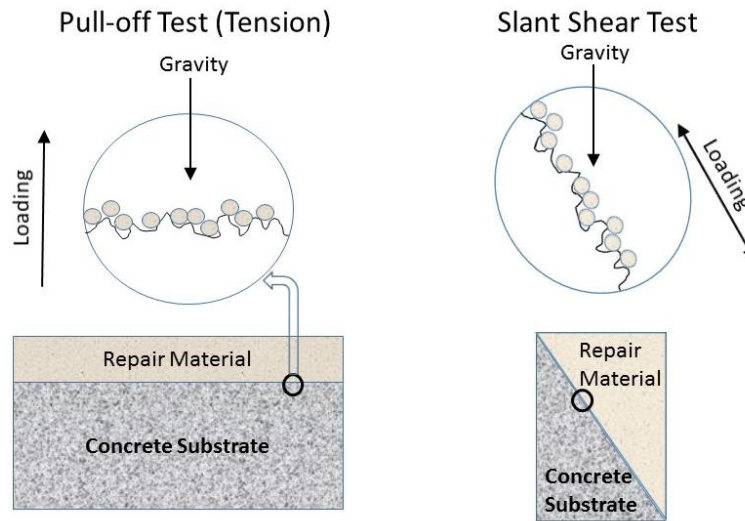


Figure 1. Schematic of differences in pull-off test vs. slant shear test with respect to directions of gravity and loading.

In pursuit of this objective, the present study includes simultaneous neutron and X-ray radiographic imaging during the hardening of a fresh RM applied to either a dry (conditioned at 50 % relative humidity [RH]) or SSD mortar substrate, with the substrate being characterized further by having either a cast or a cut top surface. X-ray absorption increases with increasing atomic number, Z , and in cement-based materials is generally proportional to the local density of the materials (solids > liquids > gas). In cement-based materials, the absorption of neutrons is mostly influenced by the presence of hydrogen atoms, with capillary pores filled with solution being the primary absorber, followed by gel hydration products. Neutron and X-ray radiography and tomography have been used in the past to examine water movement during hardening of RMs [12], salt solution absorption by dry mortars [21], the early-age drying of tile adhesive mortars [22,23], internal curing with lightweight aggregates [24,25], and interfacial transition zone (ITZ) microstructure in concrete prepared with recycled concrete aggregates of various saturation states [26], among other applications. In [12], X-ray tomography was utilized to observe microstructural changes during the hardening of a freshly applied RM. Key observations included the transport of water across the RM-existing substrate interface with a penetration of tens of mm into the substrate, and the concurrent formation of air voids within the RM near the interface. However, one caveat of their study was that the dry specimens were prepared by drying in an oven at 105 °C to a constant mass to create a “zero initial moisture content” [12], which may have induced some damage prior to the application of the RM and produced a dry material state unlikely to be encountered for a real substrate in a typical field application. Previous X-ray studies on fresh cementitious tile mortar adhesives have also indicated the growth and coalescence of air voids during the hardening/drying of these materials, when the fresh materials were exposed to a nominal 23 °C, 50 % RH environment within the X-ray microtomography chamber [23].

Another interesting observation from the tile adhesive mortar experiments in [22] is that during drying, small cement particles may be carried by the “flow” of solution that occurs towards the (top) drying surface within the specimen, so that they become concentrated at this exposed

surface. For tile adhesive mortars, this effect is exacerbated by the uncommonly high viscosity of their pore solutions (about 1 Pa·s vs. about 0.001 Pa·s for water), due to the addition of cellulose ethers and/or other viscosity-modifying admixtures [22]. This leads to the question of whether moisture transport from a RM to a dry substrate may also be accompanied by microstructural modifications within the RM near the interface, such as settling of particles and densification of the local microstructure. This topic has been considered previously by Müller and Zilch [27], who pointed out the importance of particle packing at the interface when new concrete is applied to old, based on both experimental measurements and modeling conducted using the CEMHYD3D hydration model.

Materials and Methods

During the course of this study, various specimens were prepared and evaluated at two different laboratories, namely the Federal Highway Administration (FHWA) and the National Institute of Standards and Technology (NIST). Table 1 provides a summary of the specimens and testing conditions utilized at each location.

Table 1. Summary of specimens and testing conditions employed at the two laboratories.

Specimen Type	Lab	Substrate	Substrate - dry condition	Substrate - wet condition	Test performed
Slant shear	FHWA	w/c=0.35 concrete (sandblasted surface)	50 % RH, 23 °C	Limewater 23 °C	ASTM C882/C882M-13a
Slant shear	NIST	w/c=0.4 mortar (ICRI CSP-1 & 5)	50 % RH, 23 °C	Limewater 23 °C	ASTM C882/C882M-13a
Pull-off	FHWA	w/c=0.35 concrete (aggregate exposed)	50 % RH, 23 °C	Tap water soaked for 24 h	ASTM C1583
Pull-off	NIST	w/c=0.5 concrete (smooth surface)	50 % RH, 23 °C	Wet burlap for 24 h	Draft ASTM test method (no coring)
“L” specimen of RM	NIST/NCNR	w/c=0.4 mortar (cast and cut surfaces)	50 % RH, 23 °C	Limewater 23 °C	Neutron & X-ray radiography

At the FHWA laboratory, an ordinary portland cement, ASTM C150-16 Type I/II, with a manufacturer-reported Blaine fineness of 382 m²/kg and density of 3070 kg/m³, was used to prepare a concrete with exposed aggregates to serve as the existing substrate [14], with the fine aggregate (FA) being an ordinary river sand (apparent specific gravity of 2.59) and the coarse aggregate (CA) being a dolomitic limestone (apparent specific gravity of 2.85). Dolomitic limestone aggregates have been observed to provide good bonding to paste and high strengths (compressive, flexural, and splitting tensile) and elastic modulus in both ordinary portland cement and ternary blend (cement, fly ash, and fine limestone) concretes in a recent joint NIST/FHWA study of the influence of aggregate characteristics on concrete performance [28]. For the present study, the concrete mixture was developed with a water-to-cement ratio (w/c) of 0.35 by mass, cement:FA:CA ratio of 1:1.7:2.5 (by mass), a minimum slump of 76 mm (3 in.) (achieved by using a high-range water reducer), and a targeted 28-d compressive strength of 55 MPa (8000 psi) [14]. The moisture absorptions of the fine and coarse aggregates were 1.27 % and 0.36 %, respectively; they were added to the concrete mixture in oven-dry conditions and the mix water was adjusted accordingly. Following conventional practices, a commercially-available in-form retarder was

applied to the top (cast) concrete surface so that the coarse aggregate could be easily exposed by pressure washing the concrete surface at an age of 24 h. From visual observation, the roughness obtained by this preparation method would exceed that of the profile of an International Concrete Repair Institute (ICRI) CSP-10 surface profile chip¹ (the CSP-10 having the highest roughness of the set). The concrete specimens were cured for 14 d at laboratory conditions of $23^{\circ}\text{C} \pm 2^{\circ}\text{C}$, $50\% \pm 5\%$ RH, except for the SSD specimens whose exposed aggregate surfaces were soaked with tap water during the last 24 h of the 14-d curing period, and subsequently manually dried with paper towels to provide an SSD-type surface. After the 14-d curing period, the RM were poured over the exposed aggregate concrete surface and consolidated using a manual vibrator.

Two commercially-available ‘non-shrink’ cementitious grouts were used in the study at FHWA, labelled here as RM A (“a one-component, shrinkage-compensated, fiber-reinforced product that contains an integral corrosion inhibitor”) and RM B. Each RM is supplied in a bag containing the solids fraction (e.g., cementitious materials, additives, and fine aggregates); this blend is subsequently mixed with a certain amount of water following the manufacturers’ recommendations. For grout applications, RM A requires a water-to-solids ratio (w/s) of 0.16 by mass and per the manufacturer’s specification sheet, produces a 28-d compressive strength of 62 MPa (9000 psi), whereas RM B requires a w/s of 0.17 and produces a 28-d compressive strength of 48 MPa (7000 psi).

For experiments conducted at NIST, the existing substrate consisted of a $w/c=0.4$ mortar prepared using a Type I/II ordinary portland cement, with 55 % by volume sand (a blend of four commercially available silica sands with minimal absorption). Mortar substrates were prepared in cylindrical molds, by casting against a Poly(1,1,2,2-tetrafluoroethylene) (PTFE) bottom half-specimen substrate, and demolded after 1 d. These specimens were subsequently cured in limewater for a minimum of 28 d before being used to prepare slant shear specimens with one of two RMs [10]. One day prior to the application of the RMs, the existing mortar substrates were roughened using a grinding wheel to approximately match the profile of an ICRI CSP-5 “roughness” surface profile chip. SSD substrates were returned to their limewater curing following the roughening, while dry specimens were stored in air at $23^{\circ}\text{C} \pm 2^{\circ}\text{C}$, $50\% \pm 5\%$ RH overnight. For two experiments, the mortar specimens were not roughened at all, retaining their relatively smooth cast surface (since they were cast against PTFE), visually corresponding to the roughness of an ICRI CSP-1 chip.

One of the RMs used at NIST was RM A, but with a w/s of 0.13 (repair application, measured 28-d compressive strength of 91 MPa [10]), while the other (RM C, a “one-component, pre-packaged, ready-to-use, cementitious, silica fume, fiber-reinforced, high strength shrinkage-compensated mortar”) requires a w/s of 0.135 and produces a 28-d compressive strength of 69 MPa (10000 psi). The manufacturer-reported 28-d slant shear strengths for RM A and RM C are 20.7 MPa and greater than 24.1 MPa, respectively. For a few of the RM A and RM C mixtures, internal curing was provided either via pre-wetted lightweight aggregates (LWA) or a superabsorbent polymer-coated sand (PCS), as described in detail in reference [10].

At NIST, the RMs were prepared in a three-speed planetary mixer meeting the requirements of ASTM C305 [29] by first mixing the dry powders with about 80 % of the total mixing water on low speed for 30 s and then adding the remaining water during 30 s of additional mixing on low speed. The mixing speed was immediately changed to intermediate for an additional

¹ Certain commercial products are identified in this paper to specify the materials used and the procedures employed. In no case does such identification imply endorsement or recommendation by NIST, FHWA, or SES Group & Associates, nor does it indicate that the products are necessarily the best available for the purpose.

30 s of mixing, followed by a rest period of 90 s (during the first 30 s of which the sides of the mixing bowl were scraped down) and a final mixing period of 60 s on intermediate speed [10]. The prepared materials were immediately cast into the slant shear specimen molds, with the existing mortar substrate specimens serving as the bottom half of each specimen. The slant shear specimens were demolded after 1 d and subsequently stored in a $23\text{ }^{\circ}\text{C} \pm 2\text{ }^{\circ}\text{C}$, $>98\%$ RH environment until the time of testing (at 7 d to 35 d). Slant shear testing was conducted following the protocols of ASTM C882/C882M-13a [30].

For RM C, a few pull-off test specimens were prepared at NIST as part of an evaluation of the newly proposed ASTM Standard Test Method for Evaluating the Adhesion (pull-off) Strength of Concrete Repair and Overlay Mortar. Here, a rubber mat template of 50-mm circular holes is placed on a concrete surface and 12 mm thick “hockey pucks” of the fresh RM are placed in each hole. After 1 d of curing, the rubber mat is removed and the RM pucks are tested for their pull-off strength at various ages using a commercially-available testing apparatus, without the need for coring through the RM and into the concrete substrate. The 100-mm thick concrete slab used for testing is based on an International Organization for Standardization (ISO) standard requiring a measured pull-off (cohesive) strength of at least 1.5 N/mm^2 and a 4-h surface water absorption in the range of 0.5 cm^3 to 1.5 cm^3 . Several concrete slabs meeting this specification were prepared at NIST for use with RM C and pull-off strengths were measured after 7 d and 28 d both for a dry (lab at 50 % RH) concrete substrate and for one that had been covered with wet burlap for 24 h prior to application of the RM. Since this testing was conducted on a cast concrete surface, the surface was quite smooth and would correspond to an ICRI CSP-1 or CSP-2 chip. At FHWA, pull-off (tension) testing was conducted using the same testing apparatus as at NIST, but after first coring the composite specimen through the repair layer and a sufficient depth into the substrate, as per the instructions of ASTM C1583 [31].

In addition to the slant shear specimens, small L-shaped specimens of the existing substrate mortar were prepared and cured for a minimum of 28 d to be used in the neutron and X-ray radiography experiments. For a portion of these specimens, the top 1 mm was removed using a diamond-blade laboratory saw with water as the lubricant. The cross section of these specimens measured 15 mm by 15 mm with an overall height of 35 mm and length of 23 mm (see Figure 2). After cutting some of the specimens, specimens were further divided into two groups. The first was stored in limewater at $23\text{ }^{\circ}\text{C} \pm 2\text{ }^{\circ}\text{C}$ to provide a saturated (SSD) specimen for the subsequent radiography experiments. The second was stored at $23\text{ }^{\circ}\text{C} \pm 2\text{ }^{\circ}\text{C}$ and $50\% \pm 5\%$ RH to provide a dry specimen for the radiography experiments. Samples stored in limewater gained about 1 % mass during their storage, due to water imbibition to balance the ongoing chemical shrinkage that accompanies cement hydration [32]; while those dried at 50 % RH lost about 1.5 % of their nominal 25 g mass. In comparison, for the slant shear specimens, mass gains when stored in limewater and mass losses when dried overnight were both on the order of 0.5 %.



Figure 2. Photograph of typical L-shaped specimens with surrounding PTFE form (left) and with cut top surface (right) used for the radiography experiments conducted at the NIST Center for Neutron Research.

In preparation for the application of RM C during these experiments, the top portion of each L-specimen was surrounded by thin PTFE forms, to support and seal the applied RM while minimizing both X-ray and neutron absorption (Figure 2). Prior to exposure in the neutron and X-ray beams and application of RM C, the forms were further sealed with an exterior layer of aluminum tape. After application of the RM, a piece of aluminum tape was attached loosely across the (open) top of the forms to minimize evaporation from the RM layer during the subsequent 4 h exposure in the neutron/X-ray beams. After first imaging the substrates with their attached forms (empty), RM C was prepared using the same mixture proportions as used for the slant shear specimens with a powder mass of 350 g, but using a hand (kitchen) mixer with a total mixing time of 2 min. After first resaturating the SSD mortar surface with a few drops of distilled water, this RM was applied to the top surface of both substrates to fill their forms, using a small metal spatula.

Acquisition of radiographic (through transmission) images using both neutron and X-ray sources commenced immediately after application of the RM. Two separate experiments were conducted on different days. A 4 h exposure was conducted on a pair of cut surface specimens, one SSD and the other dry (exposed to 50 % RH). On a second day, a 4 h exposure was conducted on a similar pair of specimens, but this time with cast surfaces. Details of the NIST Center for Neutron Research (NCNR) neutron imaging facility's neutron imaging procedures can be found elsewhere [21]. The present study took advantage of a newly added X-ray source that is mounted at a 90° angle with respect to the direction of the neutron beam [33]. As opposed to performing tomography (spinning the specimens), a time sequence of neutron and X-ray radiographic images was acquired, each with 30 s exposures. The X-ray source was set at a voltage of 90 kV and a power of 80 W. Images were obtained with a pixel size of 15 μm by 15 μm. Obtained images were processed, including dark and flat field corrections, registered to the empty form images, and median-filtered in sets of three using the NIFImage image analysis package [34]. ImageJ [35] was used for subsequent processing that included image division (to compare initial and final images), image rotation, histogram equalization, and color addition via a heat map lookup table.

Results and Discussion

Adhesion Testing

A summary of pull-off testing results is provided in Table 2, while those for slant shear specimens are given in Table 3. The statistical significance (t-test, 0.05 significance level) of any

differences between wet (SSD or immersed) and dry (no added moisture) conditions is indicated in a separate column in the tables. In Table 3, the measured values generally lie close to the manufacturers' specifications given earlier. While most differences are not statistically significant, the general trends indicate that SSD conditions provide higher bond strength values than dry conditions for pull-off testing, while the converse is true in 11 out of 15 cases for slant shear testing (the four cases where this was not the case are highlighted in grey in Table 3). Similar results have been presented in reference [8]. Here, it is suggested that these differences may be due to the local microstructure formed at the interface between the RM and the substrate under SSD vs. dry conditions.

Table 2. Results of pull-off testing (SSD vs. no added moisture) for various RMs

Material	Age at test (d)	SSD (MPa)	No added moisture (MPa)	$t_{0.05}$	Reference
RM A	2	2.68 ± 0.44	1.90 ± 0.40	N	[14]
	14	3.46 ± 0.50	2.77 ± 0.25	Y	
RM B	2	2.74 ± 0.42	1.82 ± 0.12	Y	
	14	3.18 ± 0.36	2.06 ± 0.57	Y	
RM C	7	0.42 ± 0.19	0.26 ± 0.03	N	Proposed ASTM test method; this study [NIST]
	28	1.13 ± 0.69	0.30 ± 0.09	N	

Table 3. Results of slant shear testing (immersed vs. dried for 24 h) for various RMs

Material	Age at test (d)	Immersed (MPa)	Dried for 24 h (MPa)	$t_{0.05}$	Reference
RM C	7	21.6 ± 5.7^A	23.9 ± 2.1	N	[10]
	35	25.6	26.3	N.A.	
RM C w/LWA	7	16.8 ± 1.0	19.5 ± 4.5	N	
	35	24.1 ± 1.6	19.3	N.A.	
RM C w/PCS	7	18.1 ± 2.2	19.4 ± 2.4	Y	
	35	19.0 ± 4.2	20.1 ± 2.2	N	
RM C (expired)	28	10.0 ± 0.9	21.0 ± 3.8	Y	this study [NIST]
RM A	7	20.2 ± 1.6	23.3 ± 2.9	N	[10]
	35	25.5 ± 0.2	30.9 ± 1.8	N	
RM A w/LWA	7	21.7 ± 0.2	24.3 ± 1.2	N	
	35	31.3 ± 0.6	28.5 ± 0.1	Y	
RM A	28	24.6 ± 1.1	33.7 ± 0.6	Y	this study [NIST]
RM A smooth (cast) surface	34	12.9 ± 0.8	11.8	N.A.	this study [NIST]
	28	11.8 ± 0.8	13.9 ± 2.0	N	
RM A sandblasted	14	14.4 ± 0.2	14.0 ± 0.7	N	this study [FHWA]

^AIndicates \pm one standard deviation for testing of two or three specimens. When no value is given, only one specimen was tested.

Figures 3 and 4 provide some direct visual evidence of these differences. As shown in Figure 3, when pull-off testing is performed, it is the wet substrate specimens that exhibit more patches of the concrete substrate remaining adhered to the repair material. Conversely, for slant shear specimens, as shown in Figure 4, one can observe isolated patches of well-adhered material on the specimens that were applied to a dry mortar substrate, while both surfaces of the slant shear specimens appear relatively free of bonded patches when the substrate is prepared under SSD

conditions. The results in Tables 2 and 3 also indicate the importance of surface roughness in increasing bonding, as the specimens prepared with a smooth (as cast) surface generally exhibited slant shear strengths that were less than $\frac{1}{2}$ of those typically obtained when manually roughening the surface to an ICRI CSP-5 profile and pull-off strengths that were significantly less than those of the exposed aggregate concrete substrate, in general agreement with the results presented in [14].



Figure 3. Photo of wet (left) and dry (right) pull-off test specimens for tests performed at NIST based on the newly proposed ASTM standard test method. The glossy white material is concrete that has adhered to the repair material specimen.

X-ray and Neutron Radiography Experiments

The X-ray and neutron radiography experiments were conducted to better understand the microstructural changes occurring at the RM-substrate interface. Processed images obtained by dividing the initial (just after the RM was applied) by the final (after 4 h of curing) image and color coding the result with a heat map lookup table (LUT) are provided in Figures 5 and 6 for the neutron and X-ray radiography results, respectively. The neutron imaging is particularly sensitive to the movement of water in these systems, while the X-ray imaging should provide a more general indication of changes in density due to both water and particle movement during the initial curing.

Figure 5 indicates significantly more water movement into the dry substrate specimen than into the SSD one for both cut and cast surfaces, as can be expected. In fact, little if any absorption of water is indicated for the SSD specimens, whether cut or cast surfaces. There is also more water movement into the cut surface specimen than into the cast surface, with the former showing a primary depth of water penetration of approximately 2.5 mm during the 4 h experiment. Within the RM itself, some minor local movement of water (wetting/drying) is indicated by the random patterns of various shades of green and blue.

Figure 6 indicates relatively minor changes in the overall density of the materials during the 4 h curing period. While the X-ray image does provide some indication of a densification near the top of the dry cut substrate specimen due to water imbibition, the water movement into it from

Dry specimens



Wet (SSD) specimens



Figure 4. Photographs of representative dry and wet specimens after slant shear testing at 28 d for RM A. In each case, the RM half specimen is on the left side of the photo. The white patches (mostly in the top images) indicate where one material has adhered to the other surface.

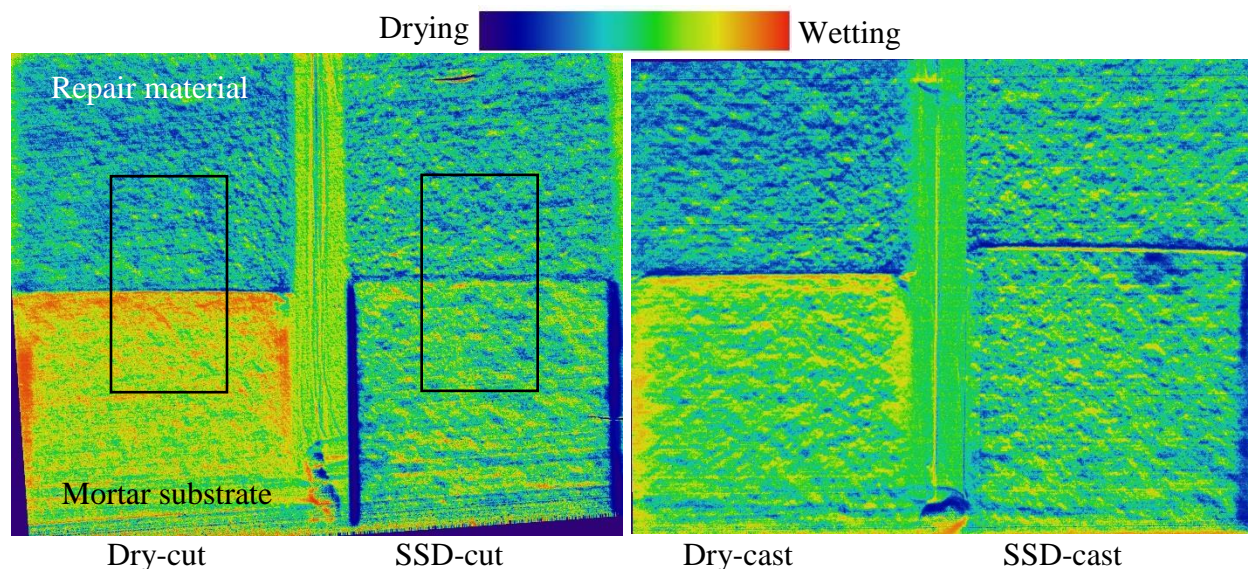


Figure 5. Processed neutron radiography images (initial divided by final) for RMs applied to mortar substrates with cut (left) and cast (right) surfaces. In each image, dry substrate is on the left and SSD one is on the right. Red/orange indicates areas where neutron absorption has increased (wetting), while dark blue indicates regions where some drying has occurred. Specimens are 15 mm wide. Boxes in center of left image indicate approximate locations of regions of interest (ROI) selected for further analysis in Figures 8 and 9.

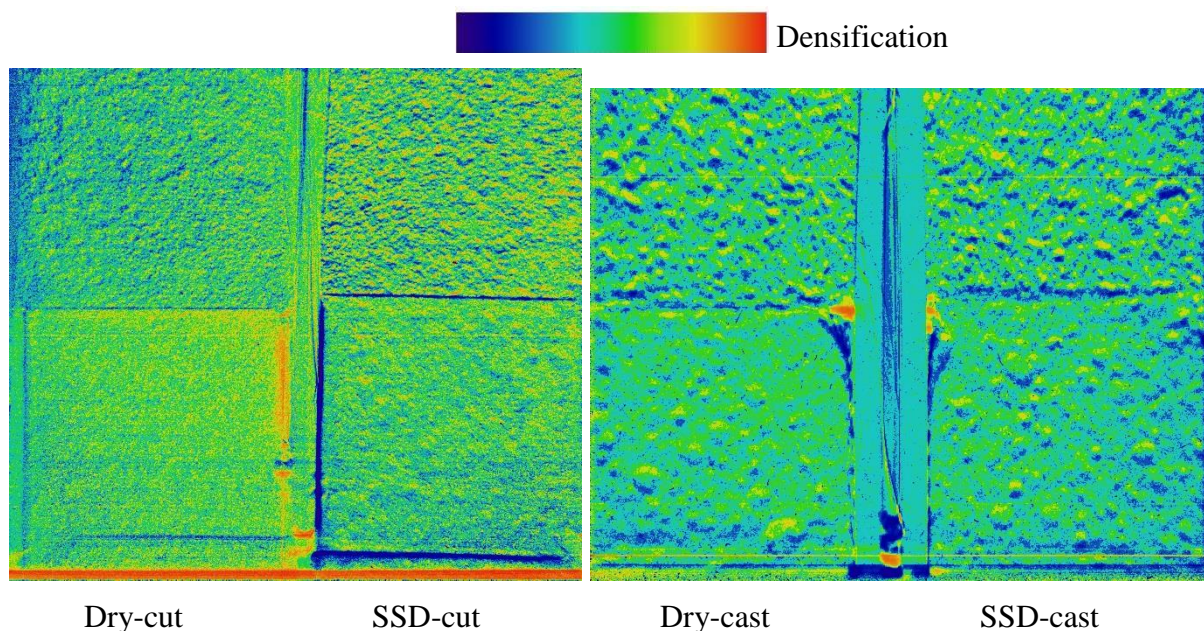


Figure 6. Processed X-ray radiography images (initial divided by final) for RMs (top) applied to mortar substrates with cut (left) and cast (right) surfaces. In each image, dry substrate is on the left and SSD one is on the right. Red/orange/yellow indicates areas where X-ray absorption has increased, which suggests densification.

the fresh RM is better detected by the neutrons (Figure 5), as water is the least dense (lowest X-ray absorption) of the non-air components of the substrate. If there is additional densification of the RM at the dry surfaces of the mortar, it is not visually apparent in the X-ray images in Figure 6, requiring further analysis of the data.

To provide an alternate view of the results, Figure 7 focuses on the cut surface specimens and shows the ratio of the empty (before RM application) to the final images for both the X-ray and neutron radiography data sets. While a random pattern of red/orange/yellow is to be expected upon application of a layer of fresh RM (increasing both neutron and X-ray absorption), there are several distinct features that violate this general pattern. At the very top surface of both specimens, there is a thin layer with a relatively high X-ray and relatively low neutron absorption signal. This likely corresponds to a layer at the top exposed surface where some drying-induced compaction has occurred, as water removal has weakened the neutron signal, while the accompanying local particle densification has increased the absorption of X-rays. For the dry-cut surface specimen, there is also an indication of a distinctly denser (and wetter) layer right at the RM-mortar interface. The measured thickness of this layer is only about 0.3 mm. Conversely, for the SSD specimen, this interface is less dense (see X-ray image in Figure 7) than the bulk of the RM, as would be expected due to parking/packing considerations at a flat surface, where a higher porosity (less dense) region with a thickness equivalent to several median particle diameters will generally exist [24,36-37]. For the dry specimen, it is hypothesized that water absorption by the dry substrate produces a layer of increased neutron absorption and the accompanying local densification of solids produces an adjacent layer of increased X-ray absorption, consistent with the images in Figure 7.

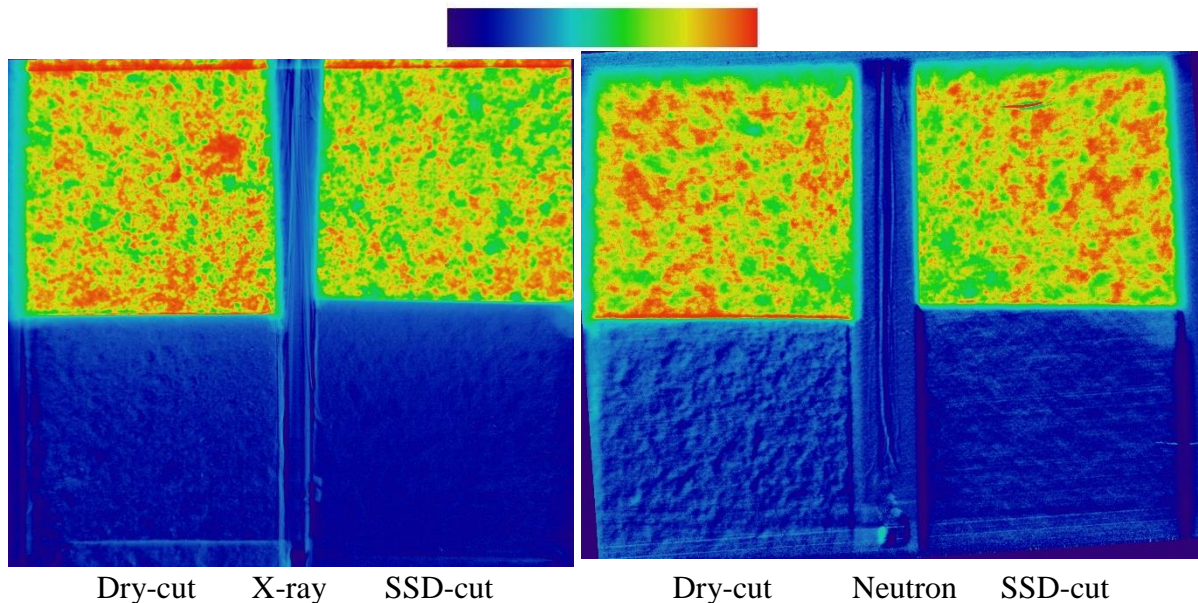


Figure 7. Processed X-ray (left) and neutron (right) radiography images (empty divided by final) for RMs (top) applied to cut mortar substrates. In each image, dry substrate is on the left and SSD one is on the right. Red/yellow/green indicates areas where X-ray or neutron absorption has increased, mainly due to the addition of the RM layer. The neutron and X-ray images were acquired at a 90 ° angle with respect to one another, prohibiting a direct one-to-one comparison.

This hypothesis is analyzed in more detail in Figures 8 and 9 which show average profile plots obtained from a central ROI region 6.5 mm wide that varied in height between 12.6 mm and 13 mm, as shown in Figure 5, of the composite specimen for the dry and SSD substrates, respectively. After image division and histogram equalization, the data values in Figure 5 range from 0 to 65,535 (16-bit image), with a midpoint value of 32,767 nominally indicating no change from the initial to the final image. The results in Figure 8 confirm the visual observations previously made from Figures 5 to 7. For the substrate, an increase in moisture content is indicated by both the neutron and X-ray profiles, with the neutrons being more sensitive (higher slope and higher values) to this wetting. For both signals, the primary wetting front extends from 6.6 mm to 9 mm, or about the same as the 2.5 mm measured on the dry cast specimen in Figure 5. However, it should also be pointed out that the signals for both neutrons and X-rays from 9 mm to 12.6 mm are well above the midpoint value of 32,767, indicating that some water has penetrated to this depth as well. Similarly, the neutron signal for the RM is well below 32,767 throughout the ROI, indicating a water loss from the entire region of the RM contained within this selected region. At early ages, water flows freely throughout the entire thickness of a thin layer of cement-based material, without the presence of the sharp (drying) front that is generally observed in hardened systems [38].

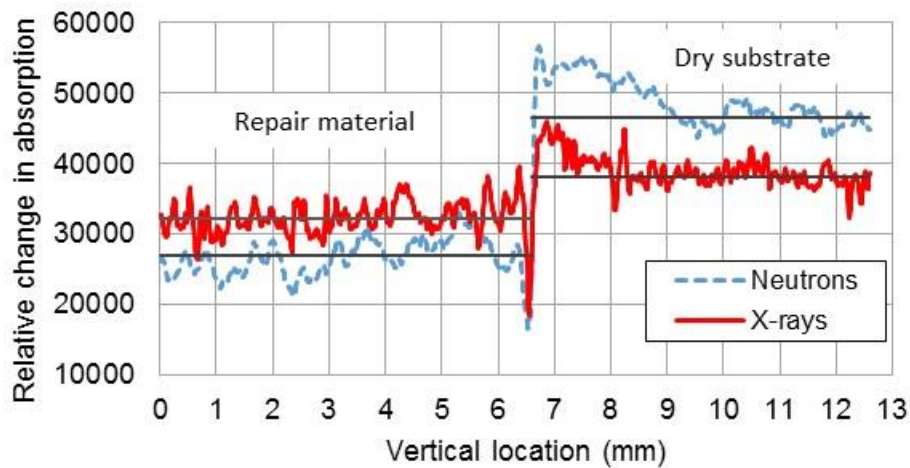


Figure 8. Profile plots for relative changes in neutron and X-ray absorption from initial application of RM until 4 h of curing. Image was 16-bit, hence signal range is from 0 to 65,535. RM(0-6.6 mm)/dry cut substrate (6.6 mm to 12.6 mm) interface is located at 6.6 mm. Solid black lines indicate the average values measured for neutrons from 0 mm to 6 mm and 9 mm to 12.6 mm, respectively, and for X-rays from 0 mm to 6 mm and 9 mm to 12.6 mm, respectively. Coefficients of variation for neutron and X-ray signals (moving across ROI) were calculated to be 20 % and 25 %, respectively.

Two more subtle trends are observed for the neutron and X-ray profiles for the RM portion of the specimen in Figure 8. For the neutron signals, greater water loss is indicated from the upper portion of the RM specimen (0 mm to 3 mm) relative to that from the lower portion (3 mm to 6 mm) within the ROI, when comparing their local signals to the “average” value indicated by one of the black lines in Figure 8. A similar analysis of the X-ray signal indicates a densification of the RM immediately adjacent to the dry substrate, specifically within about 1 mm. In this case, the neutron signal is decreasing slightly within the RM adjacent to the interface, consistent with the density increase being primarily due to the replacement of water (that was drawn into the

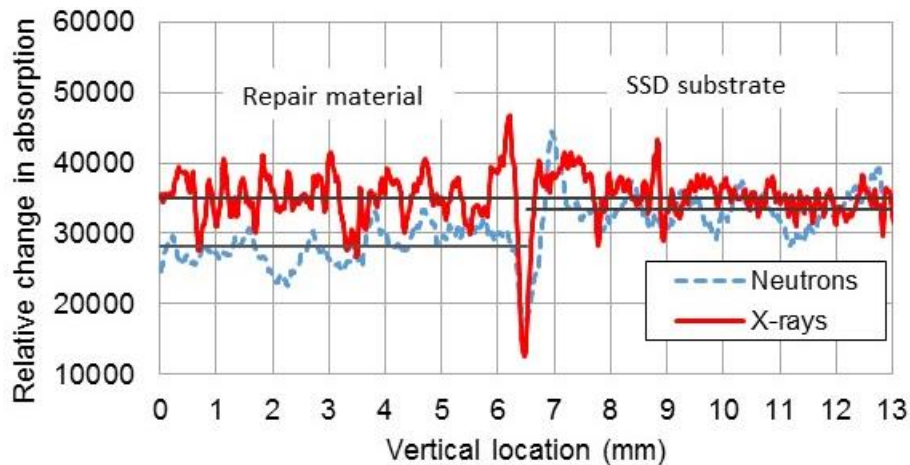


Figure 9. Profile plots for relative changes in neutron and X-ray absorption from initial application of RM until 4 h of curing. Image was 16-bit, hence signal range is from 0 to 65,535. RM/SSD cut substrate interface is located at about 6.5 mm. Solid black lines indicate the average values measured for neutrons from 0 mm to 6 mm and 8 mm to 13 mm, respectively, and for X-rays from 0 mm to 6 mm and 8 mm to 13 mm, respectively. In the latter case, these average values are nearly identical. Coefficients of variation for neutron and X-ray signals (across ROI) were calculated to be 28 % and 30 %, respectively.

substrate) by solid particles from the RM. For the case of the SSD substrate, as shown in Figure 9, there is much less difference in the neutron and X-ray signals between the RM and the substrate. The neutron data indicates that minor drying of the RM has occurred during its 4 h exposure, likely due to the sealing at the top of the PTFE/aluminum tape forms not being perfect. Basically, no change in either the density or the water content of the substrate is observed beyond a slight wetting at the very top surface. Similarly, the density of the RM is uniform except for a slight densification at the interface, consistent with a compaction of particles [24,36-37] accompanying the minor wetting of the substrate. Taken as a whole, the neutron and X-ray radiography results show that for these small mortar specimens, the microstructural rearrangement at the RM/substrate interface is quite different in the cases of dry and SSD substrates.

Scanning Electron Microscopy (SEM) Analysis

Previously, SEM analysis of the interfaces between RM and existing concrete substrates have been conducted by Beushausen et al. [13] and by De la Varga et al. [14]. In the former case, a drier substrate produced an overlay transition zone (OTZ) with lower porosity and a higher unhydrated cement content. This would imply a denser/drier interface that would be characterized by an increase in X-ray absorption and a reduction in neutron absorption, consistent with the results obtained here and presented in Figures 8 and 9. In the latter case, Figure 10 presents that group's measurements of phase fractions within the RM as a function of distance from the interface for RM in contact with only the paste portions of the concrete substrate, for both dry (Control) and SSD concrete surfaces. Clear differences are observed, with higher proportions of both unhydrated material and porosity near the interface for the dry specimen. More detailed SEM analysis has indicated that for the control specimens, some of the additional porosity at the interface is due to the presence of unfilled pores from a less than perfect consolidation of the fluid RM into the rough

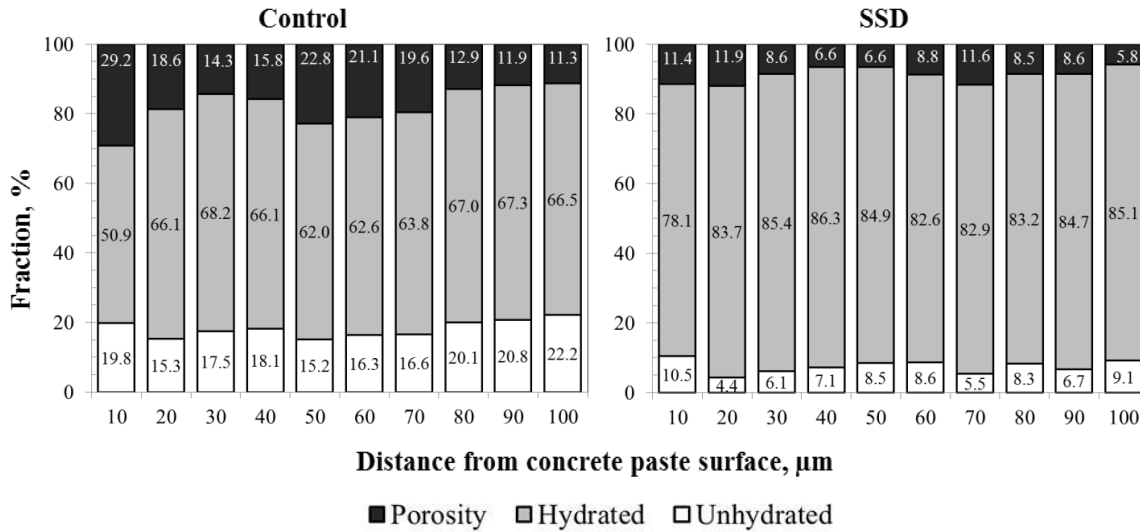


Figure 10. Porosity, hydrated, and unhydrated distribution of the RM at 14 d RM-Paste interfaces, for both control (no added moisture) and SSD specimens. (Plots are based on average measurements from three representative areas, with a coefficient of variation of below 15 %.)
From [14].

exposed aggregate concrete substrate [14]. Assuming a volumetric expansion coefficient of 2.2 for hydration products relative to the source unhydrated material [39] and that all hydration products are formed locally, Figure 11 provides a plot of the estimated initial unhydrated cement contents for the two substrate conditions (prior to any hydration). A higher initial unhydrated cement content is generally indicated for the control (no added moisture) specimen within the first 0.1 mm of the interface. While consideration of the empty porosity in the case of the control specimen would further increase the unhydrated cement within the first 20 μm or so of the interface, the difference between the control and SSD systems would still not be statistically significant given the variability in the measured data. Further SEM studies are needed under more controlled conditions (such as without the use of a retarder as was present in [14]) to confirm the working hypothesis of microstructural rearrangement when an RM is applied to a dry concrete substrate under field conditions.

The microstructural rearrangement at the interface of the RM specimen applied to a dry substrate could impact subsequent bond performance. To summarize, as moisture is absorbed by the dry substrate, the local interface microstructure in the RM is modified, as solid particles are “compacted” to locally densify the microstructure, consistent with the X-ray absorption data previously presented in reference [12]. During this densification, these particles may be drawn into valleys in the surface profile of a roughened substrate, where they will produce further filling during their subsequent hydration. In a pull-off test, solid-solid (unhydrated) contacts will not contribute substantially to the bonding, as particles that have settled into valleys will be easily withdrawn under loading, particularly when the loading is in the same direction as the one in which the settling occurred (Figure 1). In this case, the bonding level will more likely be controlled by the quantity of formed hydration products linking across the interface from the RM to the substrate, which may be greater in the case of an SSD substrate due to its enhanced water availability/hydration (Figure 10) [13,14]. However, in the case of shear loading with a sufficiently roughened surface, both hydration product and solid-solid contacts can be useful, the latter in

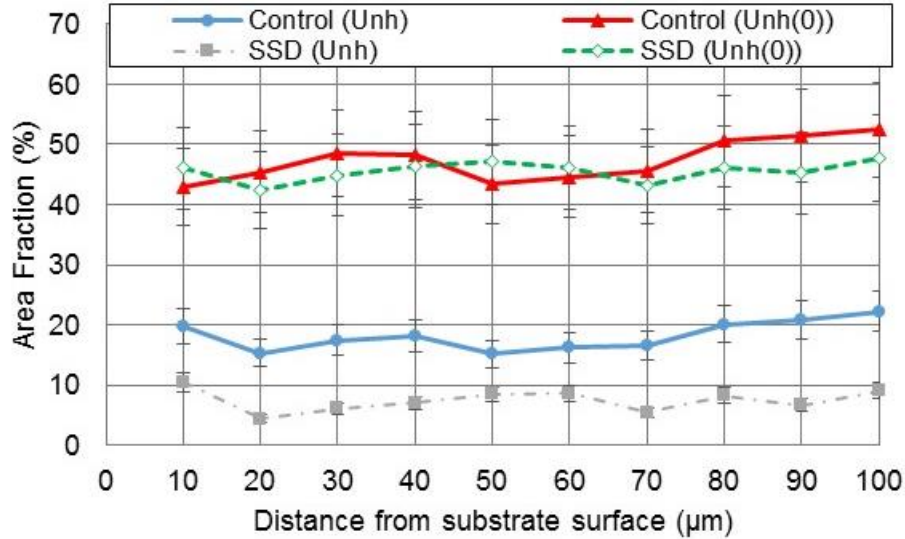


Figure 11. Plots of unhydrated phase fraction measured at 14 d and estimated at time zero (Unh(0)) based on phase fractions presented in Figure 10. Error bars represent a coefficient of variation of 15 %. Original data from [14].

generating friction that resists debonding. An analogy could be made to the bonding of Velcro, where a much greater bond is found in shear than in peel conditions, for example. This would also be consistent with the patches of bonded material observed in Figure 3 in the case of the dry substrate. The angle of the slant shear specimen may also have an influence, as gravitational settling/compaction will be occurring at a different angle than 90° with respect to the bonding surface (Figure 1). The fluidity of the RM will certainly also play an important role in this scenario, as its ability to consolidate and conform to the roughness of the surface will be critical in maximizing bond performance. Thus, at a minimum, it is the triad of RM fluidity, substrate roughness, and substrate moisture state that will be critical to engineering and optimizing bond performance in concrete structures in the field.

Conclusions

Examination of the microstructural development occurring at a RM-substrate interface using a combination of neutron and X-ray radiography has indicated that water movement and densification can be quite different in the case of a dry vs. an SSD substrate. In the former case, the flow of water from the fresh RM to the dry substrate induces significant microstructural changes that include a densification of the layer of RM immediately adjacent to the substrate. This densification provides a plausible explanation for the observation that slant shear testing with a sufficiently roughened substrate generally produces a higher measured strength when the substrate is dry prior to the application of the RM, as opposed to being moistened to SSD conditions. Conversely, for pull-off testing, SSD conditions often produce higher bond strengths, likely due to the enhanced hydration of the RM in the interfacial region via the increased availability of water. A better consolidation of the RM into the rough profile of the SSD substrate may also contribute to this enhanced bonding under tensile loading. For maximizing bond performance, detailed engineering of the RM fluidity, substrate surface roughness, and substrate moisture condition is required.

Acknowledgments

The authors would like to thank Ms. Catherine Lucero (United States Bureau of Reclamation) for her assistance in the acquisition of preliminary neutron radiography data at the NCNR neutron imaging facility and Mr. Max Peltz (NIST) for assistance with the physical testing.

References

- 1) Bissonnette, B., Vaysburd, A.M., and von Fay, K.F., “Best Practices for Preparing Concrete Surfaces Prior to Repairs and Overlays,” Report Number MERL 12-17, U.S. Department of the Interior, May 2012, 92 pp.
- 2) Bissonnette, B., Courard, L., Garbacz, A., Vaysburd, A.M., and von Fay, K.F., “Development of Specifications and Performance Criteria for Surface Preparation Based on Issues Related to Bond Strength,” Final Report ST-2017-2886-1, U.S. Department of the Interior, March 2017.
- 3) Vaysburd, A.M., Bissonnette, B., Thomassin, M.M., von Fay, K.F., Harrell, S.J., and Robertson, B., “Concrete Substrate Moisture Requirements for Effective Concrete Repairs,” Report ST-2016-2886-01, September 2016, 62 pp.
- 4) Júlio, E.N.B.S., Branco, F.A.B., and Silva, V.D., “Concrete-to-Concrete Bond Strength. Influence of the Roughness of the Substrate Surface,” *Construction and Building Materials*, Vol. 18, 675-681, 2004.
- 5) Santos, P.M.D., Júlio, E.N.B.S., Silva, V.D., “Correlation between Concrete-to-Concrete Bond Strength and the Roughness of the Substrate Surface,” *Construction and Building Materials*, Vol. 21, 1688-1695, 2007.
- 6) Beushausen, H., “The Influence of Concrete Substrate Preparation on Overlay Bond Strength,” *Magazine of Concrete Research*, Vol. 62 (11), 845-852, 2010.
- 7) Courard, L., Lenaers, J.-F., Michel, F., and Garbacz, A., “Saturation Level of the Superficial Zone of Concrete and Adhesion of Repair Systems,” *Construction and Building Materials*, Vol. 25 (5), 2488-2494, 2011.
- 8) Bissonnette, B., Vaysburd, A.M., and von Fay, K.F., “Moisture Content Requirements for Repair, Part 1: Concrete Repair Testing,” Report Number MERL-2013-63, U.S. Department of the Interior, Dec. 2014, 45 pp.
- 9) Beushausen, H., “The Influence of Precast Surface Moisture Condition on Overlap Bond Strength,” *Concrete Plant International*, Vol. 1, 144-1467, 2015.
- 10) Bentz, D.P., Jones, S.Z., Peltz, M.A., and Stutzman, P.E., “Influence of Internal Curing on Properties and Performance of Cement-Based Repair Materials,” NISTIR **8076**, U.S. Department of Commerce, July 2015.

- 11) De la Varga, I., Munoz, J.F., Bentz, D.P., and Graybeal, B.A., "Effect of the Interface Moisture Content on the Bond Performance between a Concrete Substrate and a Non-Shrink Cement-Based Grout," 2015 National Accelerated Bridge Construction Conference, Miami, FL, Dec. 7-8, 2015.
- 12) Luković, M., and Ye, G., "Effect of Moisture Exchange on Interface Formation in the Repair System Studied by X-ray Absorption," *Materials*, Vol. 9, Jan. 2016, 17 pp.
- 13) Beushausen, H., Höhlig, B., and Talotti, M., "The Influence of Substrate Moisture Preparation on Bond Strength of Concrete Overlays and the Microstructure of the OTZ," *Cement and Concrete Research*, Vol. 92, 84-91, 2017.
- 14) De la Varga, I., Muñoz, J.F., Bentz, D.P., Stutzman, P.E., and Graybeal, B.A., "Grout-Concrete Interface Bond Performance: Effect of Interface Moisture on the Tensile Bond Strength and Grout Microstructure," submitted to *Construction and Building Materials*, 2017.
- 15) Knab, L.I., and Spring, C.B., "Evaluation of Test Methods for Measuring the Bond Strength of Portland Cement Based Repair Materials to Concrete," *Cement, Concrete, and Aggregates*, Vol. 11 (1), 3-14, 1989.
- 16) Austin, S., Robins, P., and Pan, Y., "Shear Bond Testing of Concrete Repairs," *Cement and Concrete Research*, Vol. 29, 1067-1076, 1999.
- 17) Momayez, A., Ehsani, M.R., Ramezani pour, A.A., and Rajaie, H., "Comparison of Methods for Evaluating Bond Strength between Concrete Substrate and Repair Materials," *Cement and Concrete Research*, Vol. 35, 748-757, 2005.
- 18) Silfwerbrand, J., "Shear Bond Strength in Repaired Concrete Structures," *Materials and Structures*, Vol. 36, 419-424, 2003.
- 19) Rahman, A., Ai, C., Xin, C., Gao, X., and Lu, Y., "State-of-the-Art Review of Interface Bond Testing Devices for Pavement Layers: Toward the Standardization Procedure," *Journal of Adhesion Science and Technology*, 18 pp., 2016, DOI: 10.1080/01694243.2016.1205240.
- 20) Vaysburd, A.M., Bissonnette, B., and von Fay, K.F., "Compatibility Issues in Design and Implementation of Concrete Repairs and Overlays," Report No. MERL-2014-87, December 2014.
- 21) Lucero, C.L., Spragg, R.P., Bentz, D.P., Hussey, D.S., Jacobson, D.L., and Weiss, W.J., "Neutron Radiography Measurement of Salt Solution Absorption in Mortar," *ACI Materials Journal*, Vol. 114 (1), 149-159, 2017.
- 22) Bentz, D.P., Haecker, C.-J., Peltz, M.A., and Snyder, K.A., "X-ray Absorption Studies of Drying of Cementitious Tile Adhesive Mortars," *Cement and Concrete Composites*, Vol. 30, 361-373, 2008.

- 23) Bentz, D.P., and Haecker, C.-H., "X-ray Microtomography Studies of Air-Void Instability and Growth during Drying of Tile Adhesive Mortars," NISTIR **7532**, U.S. Department of Commerce, Nov. 2008.
- 24) Bentz, D.P., Halleck, P.M., Grader, A.S., and Roberts, J.W., "Water Movement during Internal Curing: Direct Observation Using X-ray Microtomography," *Concrete International*, Vol. 28 (10), 39-45, 2006.
- 25) Lura, P., Wyrzykowski, M., Tang, C., and Lehmann, E., "Internal Curing with Lightweight Aggregate Produced from Biomass-Derived Waste," *Cement and Concrete Research*, Vol. 59, 24-33, 2014.
- 26) Leite, M.B., and Monteiro, P.J.M., "Microstructural Analysis of Recycled Concrete Using X-ray Microtomography," *Cement and Concrete Research*, Vol. 81, 38-48, 2016.
- 27) Müller, A., and Zilch, K., "New Insights into Mechanisms Influencing the Bond Strength between Old and New Concrete," Congrès annuel 2008 de la SCGC, Québec, June 10-13, 2008, 10 pp.
- 28) Bentz, D.P., Arnold, J., Boisclair, M.J., Jones, S.Z., Rothfeld, P., Stutzman, P.E., Tanesi, J., Beyene, M., Kim, H., Muñoz, J., and Ardani, A., "Influence of Aggregate Characteristics on Concrete Performance," NIST Technical Note **1963**, U.S. Department of Commerce, May 2017.
- 29) ASTM International, ASTM C305-14 Standard Practice for Mechanical Mixing of Hydraulic Cement Pastes and Mortars of Plastic Consistency, ASTM International, West Conshohocken, PA, 2014, 3 pp.
- 30) ASTM International, ASTM C882/C882M-13a Standard Test Method for Bond Strength of Epoxy-Resin Systems Used with Concrete by Slant Shear, ASTM International, West Conshohocken, PA, 2013, 4 pp.
- 31) ASTM International, ASTM C1583/C1583M-13 Standard Test Method for Tensile Strength of Concrete Surfaces and the Bond Strength or Tensile Strength of Concrete Repair and Overlay Materials by Direct Tension (Pull-off Method), ASTM International, West Conshohocken, PA, 2013, 4 pp.
- 32) Bentz, D.P., "Three-Dimensional Computer Simulation of Portland Cement Hydration and Microstructure Development," *Journal of the American Ceramic Society*, Vol. 80 (1), 3-21, 1997.
- 33) LaManna, J.M., Hussey, D.S., Baltic, E., and Jacobson, D.L., "Neutron and X-ray Tomography (NeXT) System for Simultaneous, Dual Modality Tomography," *Review of Scientific Instruments*, submitted 2017.
- 34) Hussey, D., and Jacobson, D., NIFImage, Version 4.01, 2017.

- 35) ImageJ, available at <https://imagej.nih.gov/ij/>, access verified May 2017.
- 36) Ridgway, K., and Tarbuck, K.J., "The Random Packing of Spheres," *British Chemical Engineering*, Vol. **12** (3), 384-388, 1967.
- 37) Garboczi, E.J., and Bentz, D.P., "Digital Simulation of the Aggregate-Cement Paste Interfacial Zone in Concrete," *Journal of Materials Research*, Vol. **6** (1), 196-201, 1991.
- 38) Bentz, D.P., and Hansen, K.K., "Preliminary Observations of Water Movement in Cement Pastes During Curing Using X-ray Absorption," *Cement and Concrete Research*, Vol. **30** (7), 1157-1168, 2000.
- 39) Snyder, K.A., and Bentz, D.P., "Suspended Hydration and Loss of Freezable Water in Cement Pastes Exposed to 90 % Relative Humidity," *Cement and Concrete Research*, Vol. **34** (11), 2045-2056, 2004.